Climate Dynamics (2019) 52:1443–1459
https://doi.org/10.1007/s00382-018-4206-3

Future changes in Asian summer monsoon precipitation extremes as inferred from 20-km AGCM simulations

Yuk Sing Lui[1] · Chi-Yung Tam[1] · Ngar-Cheung Lau[2,3]

Received: 23 June 2017 / Accepted: 5 April 2018 / Published online: 17 April 2018

Abstract
This study examines the impacts of climate change on precipitation extremes in the Asian monsoon region during boreal summer, based on simulations from the 20-km Meteorological Research Institute atmospheric general circulation model. The model can capture the summertime monsoon rainfall, with characteristics similar to those from Tropical Rainfall Measuring Mission and Asian Precipitation-Highly-Resolved Observational Data Integration Towards Evaluation. By comparing the 2075–2099 with the present-day climate simulations, there is a robust increase of the mean rainfall in many locations due to a warmer climate. Over southeastern China, the Baiu rainband, Bay of Bengal and central India, extreme precipitation rates are also enhanced in the future, which can be inferred from increases of the 95th percentile of daily precipitation, the maximum accumulated precipitation in 5 consecutive days, the simple daily precipitation intensity index, and the scale parameter of the fitted gamma distribution. In these regions, with the exception of the Baiu rainband, most of these metrics give a fractional change of extreme rainfall per degree increase of the lower-tropospheric temperature of ~5 to 8.5% K^{-1}, roughly consistent with the Clausius–Clapeyron relation. However, over the Baiu area extreme precipitation change scales as ~3.5% K^{-1} only. We have also stratified the rainfall data into those associated with tropical cyclones (TC) and those with other weather systems. The AGCM gives an increase of the accumulated TC rainfall over southeastern China, and a decrease in southern Japan in the future climate. The latter can be attributed to suppressed TC occurrence in southern Japan, whereas increased accumulated rainfall over southeastern China is due to more intense TC rain rate under global warming. Overall, non-TC weather systems are the main contributor to enhanced precipitation extremes in various locations. In the future, TC activities over southeastern China tend to further exacerbate the precipitation extremes, whereas those in the Baiu region lead to weaker changes of these extremes.

1 Introduction

Climate change can bring great impacts on the society by changing both the frequency and intensity of extreme events. Many studies have been devoted to understanding how global warming might influence the characteristics of extreme precipitation, both in the global (e.g., Frich et al. 2002; Groisman et al. 2005; Alexander et al. 2006; Lau and Wu 2007; Zhang et al. 2011) and the regional/local perspectives (Qian and Lin 2005; Wang and Zhou 2005; Zhai et al. 2005; Chen et al. 2007). Researchers have also made use of climate models to project future changes in intense rainfall (Sun et al. 2007; Sillmann and Roeckner 2008; Jiang et al. 2012; Sillmann et al. 2013). Under a warmer background climate, precipitation extremes is expected to increase at a rate much faster than the globally-mean precipitation (Easterling 2000; Meehl et al. 2000; Allen and Ingram 2002; Donat et al. 2016). According to the Clausius–Clapeyron (CC) relation, the atmospheric moisture-holding capacity increases by about 7% per degree K increase in the lower-tropospheric temperature. Although the CC relation is useful for scaling precipitation extremes (Pall et al. 2007), other dynamic factors such as changes in the upward velocity may also be

Electronic supplementary material The online version of this article (https://doi.org/10.1007/s00382-018-4206-3) contains supplementary material, which is available to authorized users.

✉ Chi-Yung Tam
Francis.Tam@cuhk.edu.hk

[1] Earth System Science Programme, The Chinese University of Hong Kong, Hong Kong, China

[2] Institute of Environment, Energy and Sustainability, The Chinese University of Hong Kong, Hong Kong, China

[3] Department of Geography and Resource Management, The Chinese University of Hong Kong, Hong Kong, China

important for considering the impact of global warming on intense rainfall (e.g. Emori and Brown 2005; IPCC 2012). In fact, super-Clausius–Clapeyron scaling of sub-daily precipitation extremes in Europe and Japan have been reported (Lenderink and van Meijgaard 2008; Fujibe 2013).

It is well known that tropical cyclones (TC) can lead to very intense local precipitation. Over the western north Pacific (WNP) basin, TCs contribute significantly (about 11%) to the total rainfall during the peak TC season (Jiang and Zipser 2010). In general, most climate models tend to underestimate the TC genesis frequency over WNP, particularly during July-to-September season (e.g. Yokoi et al. 2009). In the global mean sense, projections using high-resolution models give an increase (decrease) of TC intensity and TC (frequency) by 2–11% (6–34%) at the end of twenty-first century (Knutson et al. 2010). Reductions in the global as well as the hemispheric mean TC numbers are probably robust and independent of model physics (Murakami et al. 2012). On the other hand, future changes of TC activity and TC-related rainfall for individual basins remain uncertain (Sugi et al. 2009; Knutson et al. 2010; Murakami et al. 2012). Several studies have identified a reduction of TC frequency in the western North Pacific (WNP) in the globally-warmed future (Yokoi et al. 2009; Murakami et al. 2011), while others project an insignificant change (Manganello et al. 2014). A recent study by Kossin et al. (2016) shows that TC frequency in WNP is projected to decrease by analyzing explicitly generated TCs in model outputs, but the same quantity will increase if a dynamical downscaling method suggested by Emanuel (2013) is used instead. Chang et al. (2012) studied intense rainfall due to non-TC systems, and those related to TCs and their passages, and found that their trends can be drastically different. It is still unclear how extreme rainfall in the Asian monsoon region might be affected by TCs in the future climate.

Recently, Mizuta et al. (2012) and Murakami et al. (2012) examined the performance of the 20-km resolution atmospheric general circulation model of Meteorological Research Institute (MRI-AGCM3.2S) in capturing the Asian monsoon circulation as well as TC activities. The high-resolution AGCM is capable of simulating local features such as orographic precipitation (e.g. over Taiwan and Philippines), and large-scale phenomena such as the Asian summer monsoon. The model can also give realistic TC circulation and precipitation, TC occurrence frequency and its interannual variability in WNP (Murakami et al. 2012). More recently, Kitoh and Endo (2016a) and Kusunoki (2017b) also showed that this AGCM has good skills in simulating extreme rainfall in a global sense. Motivated by these results, this study makes use of the same AGCM to further examine the impact of global warming on regional rainfall statistics over the Asian monsoon region, with a primary focus on precipitation extremes. Yun et al. (2008) suggested that not only the enhanced precipitable water but other factors (e.g. TC activity) also contribute to the extreme precipitation changes under warming climate. Thus, this study also investigates whether extreme precipitation over various Asian monsoon sub-regions scales according to the CC relation, and examines the relative contribution of TC and non-TC weather systems to extreme precipitation. The remainder of this paper is organized as follows. Section 2 briefly introduces the model experiments and datasets used. Section 3 assesses the performance of the AGCM in reproducing the daily precipitation statistics in the Asian monsoon region as well as the TC climatology in the WNP basin. Sections 4 and 5 give the projected changes of precipitation extremes and TC-related rainfall statistics. Discussions and summary are given in Sect. 6.

2 Model experiments and methodology

2.1 AGCM experiments

The MRI-AGCM3.2S is based on the global spectral model developed by MRI of the Japan Meteorological Agency (JMA), and has been used for projecting the future climate, daily precipitation extremes and TC activity. It is a hydrostatic, primitive-equation model at the TL959 resolution (corresponding to a grid size of ~ 20×20 km) with 64 unevenly-spaced vertical levels reaching 0.01 hPa. The radiation scheme from the JMA operational model is used (JMA 2007), while cumulus convection is parameterized based on a mass-flux scheme (Yukimoto et al. 2011). The planetary boundary layer and the land surface are represented by the Mellor and Yamada (1974) scheme and the new Simple Biosphere (New-SiB) land surface model (Hirai et al. 2007), respectively. More detailed descriptions of this model were given by (Mizuta et al. 2012). To realize the present day (PD) climate in this model, the AGCM was integrated with the Hadley Centre (Rayner et al. 2003) monthly-mean sea surface temperature (SST) and sea ice concentration observed from 1979 to 2003. For the future globally-warmed (GW) climate, the averaged SST and sea ice projections by 18 models for the 2075–2099 period were used as the lower-boundary forcing (Murakami et al. 2012). These model projections were produced under the Special Report on Emissions Scenarios (SRES) A1B scenario, for the Coupled Model Intercomparison Project phase 3 (CMIP3) (Solomon et al. 2007).

In order to evaluate the performance of the MRI AGCM in capturing the Asian monsoon circulation and TC activities, various observational and reanalysis products were used in this study. Here the precipitation products from the Tropical Rainfall Measuring Mission 3B42 version 7 (TRMM3B42v7) (Huffman et al. 2007) and the Asian

Precipitation-Highly-Resolved Observational Data Integration Towards Evaluation version 1101 (APHRODITEv1101) for monsoon Asia (Yatagai et al. 2012) were selected for this purpose. The TRMM3B42 daily accumulated rainfall dataset provides daily precipitation rate estimates at the 0.25°×0.25° resolution, based on measurements from multiple satellites for the period of 1998–2013. The APHRODITE dataset, which is produced by interpolating rain gauge observations, provides gridded daily precipitation rate over land within 0°–55°N, 60°–150°E, for the 1979–2003 period. Many studies have used this gauge-based dataset for studying the mean precipitation (Xie et al. 2007; Sohn et al. 2012) and extremes (Kamiguchi et al. 2010). Zhao and Yatagai (2014) analyzed the rain gauge record (by adopting a gauge data analysis algorithm from APHRODITE) over Chinese stations and found that the TRMM3B42v6 (a version older than that used in this study) rainfall estimates agree well with the gauge data, except with underestimations in western China. Also, they found that TRMM3B42 tends to overestimate extreme daily precipitation over the southeastern China and underestimate moderate precipitation over the northwestern China. The Joint Typhoon Warning Center (JTWC) best track data for TCs in WNP were also used. Note that only TCs with maximum 1-min-sustained wind speed of 18 m s^{-1} or greater (i.e. tropical storm intensity) were considered. Finally, upper-air meteorological variables such as winds and temperature from the Japanese 55-year Re-Analysis (JRA-55; Kobayashi et al. 2015) monthly data were also used for model evaluation.

2.2 Methods for quantifying precipitation extremes

To assess the AGCM's performance in capturing extreme events and to quantify their changes, three commonly used indices were adopted to characterize intense rain rates. They are (i) the simple daily precipitation intensity index (SDII), which is defined as the accumulated precipitation divided by the number of rain days over a particular period of time, (ii) the 95th percentile of daily precipitation during wet days (Prec95p), and (iii) the maximum accumulated precipitation in 5 consecutive days (R5d). Throughout this study, wet (dry) days are defined as days with accumulated precipitation above (below) 0.1 mm. Besides using these empirical indices, we have also investigated the use of the parametric gamma distribution to characterize the daily mean precipitation during wet days. The two-parameter gamma distribution function is given by

$$f(x) = \frac{1}{\beta^{\alpha}\Gamma(\alpha)} x^{\alpha-1} e^{-x/\beta}, \quad x, \alpha, \beta > 0 \tag{1}$$

where x is the daily precipitation during wet days, α and β are the shape and scale parameters respectively, and Γ(α) is the gamma function. The dimensionless α parameter characterizes the shape of the gamma distribution. When $\alpha < 1$, the probability distrubution function (PDF) is a hyperbolically decreasing distribution; when $\alpha = 1$, it becomes an exponential function; in the limit of $\alpha \to +\infty$, it approaches a normal distribution. The parameter β represents the spread of the distribution, and can be interpreted as a measure of the variability of the daily mean precipitation. It is widely recognized that the gamma distribution provides a reasonably good fit to the observed and also model-simulated daily precipitation (Groisman et al. 1999; Semenov and Bengtsson 2002; Wilby and Wigley 2002). Cho et al. (2004) reported that the PDF of daily precipitation rates from TRMM could be well represented by the gamma distribution, especially in wet regions. The parameters α and β can be estimated using the method of maximum likelihood. To test the goodness of fit of the gamma distribution, the K–S test was applied in this study. It is used to test the null hypothesis that the data comes from a theoretical distribution function, based on the maximum difference between the empirical and theoretical cumulative distribution functions (CDF):

$$D_n = \max_x \left| F_n(x) - F(x) \right| \tag{2}$$

where $F_n(x)$ is the empirical CDF for a dataset with a sample size n and $F(x)$ is the theoretical CDF. The null hypothesis is rejected at a given significance level if the statistics exceed a critical value in a standard table. In general the shape parameter is spatially and temporally more stable compared to the scale parameter (Groisman et al. 1999; Semenov and Bengtsson 2002; Wilby and Wigley 2002). Here the scale parameter is included as one of the precipitation indicators in this study.

2.3 Deducing TC rainfall

We have also performed analysis of precipitation due to TC occurrences. Here TCs are tracked by the algorithm similar to that used by Murakami et al. (2012), which is based on 6-hourly AGCM outputs. A TC-like system in the model is identified whenever: (1) the local maximum 850 hPa vorticity exceeds 2.0×10^{-4} s^{-1}; (2) the local maximum wind speed at 850 hPa exceeds 17.0 m s^{-1}; (3) the sum of maximum temperature deviations at 300, 500 and 700 hPa exceeds 2.0 K, with the deviation defined as the departure from temperature averaged over a 10°×10° box centered at the position of maximum 850 hPa vorticity; (4) the maximum 850 hPa wind speed is larger than that at 300 hPa; and (5) the lifetime of the system must be 36 h or more and the genesis must happen over the ocean. TC frequency (TCF) is defined as the total count of TC occurrences within each 5°×5° grid box for every 6 h. The first detected position is defined as the TC genesis location, except at the boundaries of the study domain. TC genesis frequency is also

defined similarly to TCF. (For observations, TCF and TGF are defined in the same way based on JTWC 6-hourly best track data, for TCs reaching the tropical storm intensity; see Sect. 2). Finally, based on the positions of identified TCs at every 6 h, we can further stratify precipitation over each grid box into TC and non-TC related rainfall. According to criteria suggested in previous studies (e.g. Jiang and Zipser 2010; Guo et al. 2017), rainfall within 5° (i.e. roughly 500 km) from the TC center is considered to be associated with TCs. This way, 6-hourly precipitation can then be converted into TC and non-TC related precipitation, in which the latter denotes the precipitation related to other non-TC weather systems such as monsoon and frontal systems.

3 Model simulations of present-day precipitation characteristics

Before examining the impact of global warming on precipitation characteristics, the capability of the MRI AGCM in capturing the summertime circulation and precipitation over the Asian monsoon area is first assessed. Figure 1 shows the May-to-September (MJJAS) climatological mean precipitation rates computed from TRMM, as well those based on model simulations for the present climate. It can be seen that the AGCM can capture well the major monsoon rain features in this region, such as the western north Pacific Intertropical Convergence Zone (ITCZ), rainfall over BOB and the Indian subcontinent, and the Baiu rainbelt. It is noteworthy that orographic precipitation such as that over the Western Ghats, the foothill of Himalayas and the Philippines are also well reproduced by the model. On the other hand, values over southeastern China (east of Japan) appear to be overestimated (underestimated). The precipitation rate averaged over 0°–50°N, 60°–150°E is about 5.84 mm day^{-1}, which is comparable to that based on TRMM for the same area (~5.50 mm day^{-1}). Also shown in Fig. 1 are the corresponding 850 hPa wind fields from JRA55 and those based on the AGCM run, for the same period of 1997–2003. The climatological mean low-level circulation is also reasonably captured by this model. Indeed, the simulated wind branches associated with the Indian and East Asian monsoon systems match well with those depicted in the JRA55 climatology. We have also examined the month-to-month evolution of the precipitation field in the same domain. The AGCM can produce the seasonal progression of the Asian monsoon, including its onset during May in BOB, the emergence of the monsoon rainband in SCS and Meiyu region, and a monsoon break in August (see Fig. S1). However, it was also found that the AGCM cannot capture the migration of the monsoon rainband into the Baiu region; its northward extension in the model is limited to around 35°N (see Fig. S2). Similar biases were reported in previous studies (e.g. Kusunoki 2016).

In addition to assessing the AGCM seasonal mean circulation and precipitation, we have compared model simulated precipitation extremes with observations. Figure 2 compares the R5d based on AGCM simulations for the present climate, with values computed using TRMM and the APHRODITE datasets. From TRMM (and to a lesser extent APHRODITE), it is seen that the geographical distribution of R5d bears much similarity with the mean precipitation pattern in the Asian monsoon area. In general, locations with intense daily mean rainfall are collocated with those having large seasonal averages in summer. The MRI AGCM data reflect this phenomenon, and indicate extreme daily precipitation rates over the Western Ghats, the BOB region, central to southern SCS west of the Philippines and south of Japan. Compared with TRMM, the model simulated R5d is underestimated, with a negative bias of 3.95 mm over SEA and EA monsoon; the same comparison with APHRODITE, however, gives

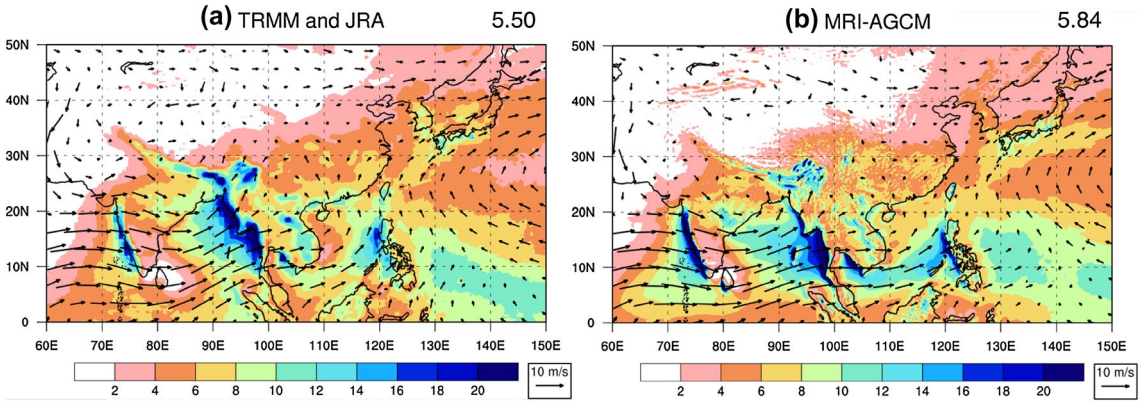

Fig. 1 Climatological mean daily precipitation rate (shading; units: mm day^{-1}) and 850 hPa winds (see scale arrow at bottom right) over MJJAS based on **a** TRMM3B42v7 and JRA55 data for the 1998–2013 period, and **b** MRI-AGCM3.2S outputs for the period of 1979–2003. The precipitation rate averaged over the domain of 0°–50°N, 60°–150°E is shown in upper right corner of each figure

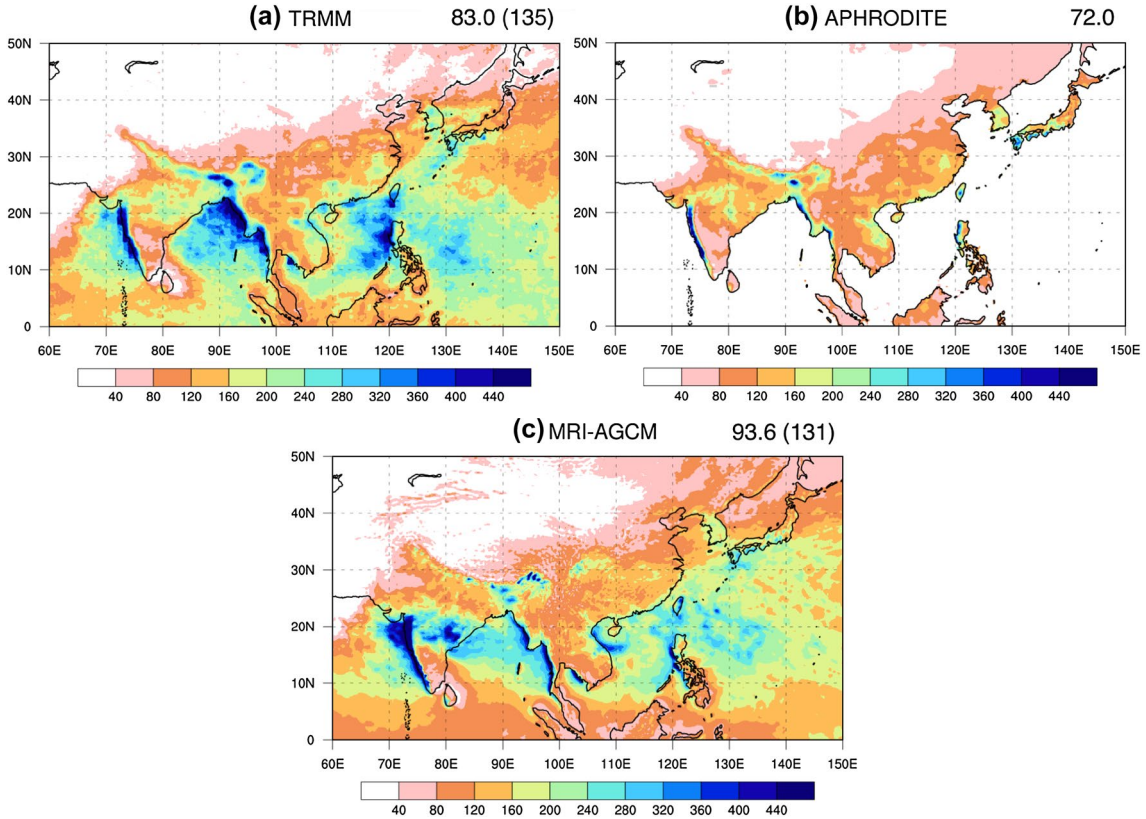

Fig. 2 R5d (units: mm) for MJJAS computed based on **a** TRMM3B42v7 for the 1998–2013 period, **b** APHRODITEv1101, and **c** MRI-AGCM3.2S for the 1979–2003 period. The R5d value averaged over the land area of the domain of 0°–50°N, 60°–150°E is shown in the upper right of each panel; for TRMM3B42v7 and MRI-AGCM3.2S, the same quantity is computed over both land and sea, and is also shown (see number in parentheses)

an overestimation of 21.6 mm. Finally, the pattern correlation between AGCM and observed R5d (either TRMM- or APHRODITE-based) is about 0.8. Table 1 summarises the performance of the AGCM in simulating various measures of precipitation characteristics, by giving the pattern correlation coefficient, mean bias and root-mean-square error of the seasonal mean, SDII, R5d and Prec95p when compared with observational datasets. Consistent with previous works

Table 1 Pattern correlation coefficient (PCC), mean bias, and root-mean-square error (RMSE) between daily precipitation statistics from MRI-AGCM and TRMM3B42v7 over the domain of 0°-50°N, 60°-150°E, and that between model and APHRODITEv1101 over land area in the same domain

	Seasonal mean	SDII	R5d	Prec95p
Definition	Precipitation total divided by number of days	Precipitation total divided by number of wet days	Maximum 5-day precipitation amount	The 95th percentile of the set of the daily precipitation in wet days
TRMM3B42v7 (MJJAS, 1998–2013)				
PCC	0.867	0.791	0.840	0.756
Mean bias	0.343 mm day^{-1}	− 3.29 mm day^{-1}	− 3.93 mm	− 17.6 mm day^{-1}
RMSE	2.03 mm day^{-1}	4.55 mm day^{-1}	51.1 mm	21.5 mm day^{-1}
APHRODITEv1101 (MJJAS, 1979–2003)				
PCC	0.840	0.817	0.849	0.805
Mean bias	0.785 mm day^{-1}	1.14 mm day^{-1}	21.6 mm	1.54 mm day^{-1}
RMSE	2.22 mm day^{-1}	2.51 mm day^{-1}	46.1 mm	7.72 mm day^{-1}

(e.g. Endo et al. 2012; Kusunoki 2016), it was found that the AGCM has good skills in capturing the observed climatological large-scale patterns of these metrics, with pattern correlation coefficients ranging from 0.76 to 0.87.

Besides validating the AGCM's reproducibility of mean and extreme precipitation, we have further assessed the ability of the AGCM in reproducing TC activity and more importantly TC-related precipitation in boreal summer. Figure 3 shows the observed and model simulated TCF in the WNP basin in MJJAS. Observations indicate a region with the most frequent TC occurrences over and to the east of the Luzon Strait, with an average of 12.5 TCs found in WNP during the MJJAS season. It is obvious that the model can reproduce well both the TCF pattern and also the total storm number per season (11.9 TCs). Inspection of the observed TC genesis in WNP reveals two peaks located in SCS and east of the Philippines; As mentioned in Sect. 1, underestimation of genesis frequency over WNP is found in many climate models (e.g. Yokoi et al. 2009). Despite having a very similar distribution, the MRI AGCM also underestimates the genesis frequency, particularly in the SCS region (figure not shown).

We have also computed the fraction of TC rainfall to total accumulated rainfall in MJJAS from this AGCM (see Fig. S3). Its geographical distribution and the basin-wise area-averaged value (0.102) are very consistent with those given by Jiang and Zipser (2010) (who focused on the JJASON season). Based on the TRMM-3B42 dataset, they found that the area-averaged fraction of TC rainfall to total rainfall in WNP is about 0.11. Given that the magnitude and distribution of simulated mean precipitation and ratio of TC rainfall to total rainfall are close to the observed ones, overall assessments indicate that the model can give fairly realistic TC behavior and precipitation (both TC and non-TC related) over the Asian monsoon and WNP regions. Next, we shall infer the impact of global warming on summertime precipitation extremes and TC-related rainfall based on future climate projections from this AGCM.

4 Future projected changes in precipitation intensity

Changes of the seasonal mean monsoon circulation are first examined, by comparing the model GW and PD simulations. Figure 4 shows the GW minus PD MJJAS mean precipitation rates, 850 hPa wind fields and surface air temperature using these AGCM runs. It can be seen that the seasonal mean rainfall will be enhanced over many locations in South and East Asia. Robust increase is found over BOB, the western Pacific ITCZ and some of the marginal sea areas, the Meiyu-Baiu rainbelt, Central India, the eastern and also northeastern part of China. On the other hand, there are insolated regions where the seasonal mean rainfall will be reduced under global warming. In particular, an anomalously dry zone extending from coastal Vietnam to WNP can be inferred. Precipitation rates over the Western Ghats are also reduced. Overall, the mean rain rate averaged over 0°–50°N, 60°–150°E is projected to increase by 0.34 mm day^{-1} near the end of the twenty-first century. Changes in the low-level wind take the form of an anomalous anti-cyclone over WNP, while easterly anomalies are found over the tropical Indian Ocean and central-to-southern SCS. These suggest a slightly weakened Asian summer monsoon wind circulation, especially over the Indian monsoon region, but heavier rainfall in the GW climate, consistent with many previous works (e.g. Vecchi and Soden 2007). For the surface air temperature, there is an increase over all locations in the Asian monsoon domain. The surface warming is stronger over land than over the ocean, and its signal tends to be greater over the Tibetan

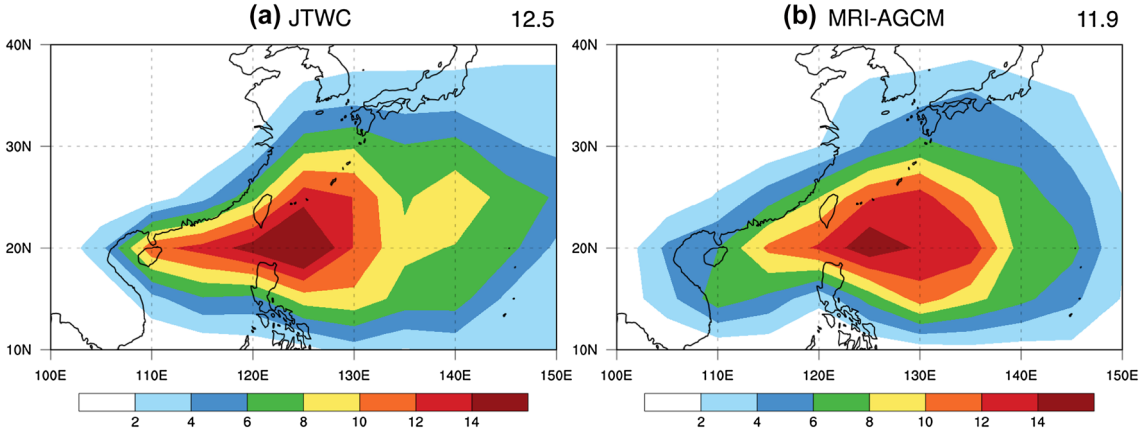

Fig. 3 TC occurrence frequency per season over each 5°×5° grid box in MJJAS based on **a** JTWC best track data, and **b** MRI-AGCM3.2S simulations. Statistics are computed for the 1979–2003 period. The average number of TCs generated per year over the domain of 0°–50°N, 60°–150°E is shown in upper right corner of each figure

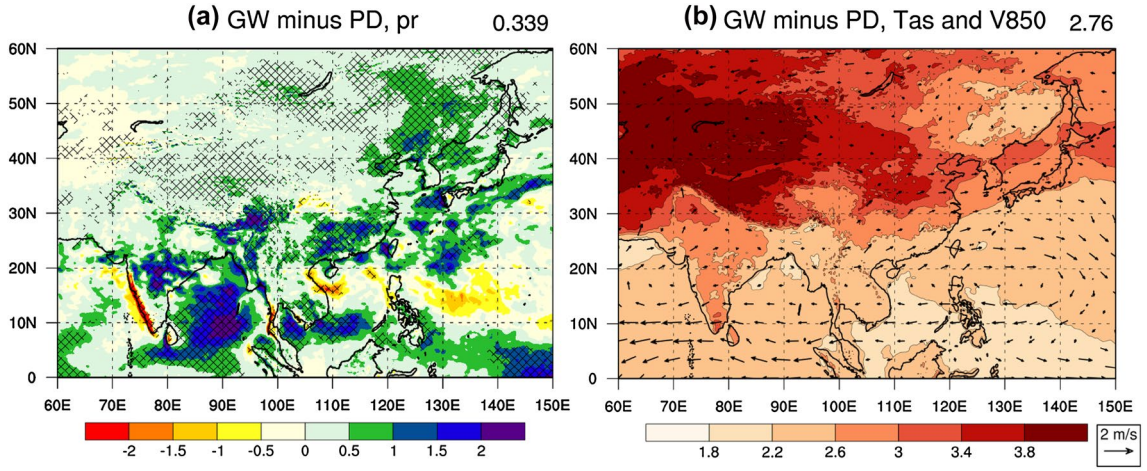

Fig. 4 Globally-warmed minus present-day **a** daily mean precipitation rate (units: mm day^{-1}), and **b** mean surface air temperature (units: K) averaged over MJJAS based on MRI-AGCM simulations. Their averaged values over the domain of 0°–60°N, 60°–150°E are shown in the upper right of each panel. Cross-hatches in **a** indicate that the differences pass the 90% significance level based on the two-sided Student's t test. Also shown in **b** are the MJJAS mean of globally-warmed minus present-day 850 hPa winds (see scale arrow at bottom right)

Plateau, and in high-latitude regions such as northern China and Mongolia. The model gives a 2.76 (2.98) K increase in the MJJAS mean surface (lower-tropospheric) air temperature over Asia by the end of the twenty-first century.

We now focus on future changes in extreme precipitation given by the AGCM simulations. Figure 5a–c show the GW minus PD values of SDII, R5d and Prec95p respectively. It is noteworthy that they were found to increase significantly over locations where the mean rainfall also increases (see Fig. 4a). In particular, four regions with a coherent increase of both the mean and extreme precipitation can be identified, namely southeastern China (22–32N, 108–122E), Baiu rainband (30–35N, 125–145E), BOB (6–17N, 85–95E), and central India (17–22N, 74–82E). We have also computed changes of the scale parameter, which is used for characterizing the gamma-fitted daily precipitation (see Sect. 2). Figure 5d gives the GW minus PD values of the scale parameter over locations where the gamma distribution can well represent the daily rainfall PDF. The goodness of fit was assessed by first carrying out the K–S test, for each summer from 1979 to 2003. The gamma distribution is then assumed to be valid if, at a particular location, there is 80% (or more) of summer seasons during which the test reaches the 10% significance level. Out of these four abovementioned regions, two of them (southeastern China and BOB) indicate a positive change of the scale parameter. Overall, the above suggests a robust increase of both the seasonal mean and daily extremes of precipitation over these four sub-domains, due to the influence of global warming. The area-averaged values of these projected changes are listed in Table 2. Increase in both the seasonal mean precipitation and extremes are statistically significant at the 99.9% level. Changes in the mean precipitation (Prec95p) averaged over southeastern China, Baiu rainband, BOB and central India are 0.718 (3.57), 0.660 (4.31), 1.58 (5.77) and 1.24 (6.89) mm day^{-1}, respectively. The corresponding percentage changes of the mean (Prec95p) are 4.45 (4.68), 3.33 (3.32), 5.36 (6.42), 6.12 (8.47) % K^{-1}, respectively. Note that there is a discrepancy between the magnitudes of changes in the mean and extreme indices; this is in accordance with other studies, which show that the far tail of the daily precipitation PDF tends to extend more to higher values compared to the mean, causing the PDF to become more right-skewed under the influence of global warming (e.g. Allen and Ingram 2002).

From the four regions considered above, the PDFs of area-averaged daily precipitation rates generated from the AGCM are further examined. Figure 6 give the results computed based on the PD and GW experiments. Also shown are the observed PDFs based on TRMM (for all four regions) and APHRODITE (for southeastern China and central India only) datasets for comparison. Consistent with the results for SDII and Prec95p, TRMM (see red dashed curves) tends to give stronger daily extreme in comparison with the AGCM (blue curves). On the other hand, the model generated PDFs appear to be consistent with those estimated using the APHRODITE datasets over land (see brown dashed curves). Regarding the influence of global warming, it can be inferred that the probability of extreme rainfall is enhanced in the GW model environment, compared to the PD simulations. Such increment in the heavy precipitation likelihood is especially obvious for daily rain rates of about 30 mm day^{-1} or more. In fact, the probability of 30–40 mm day^{-1} events is projected to increase by about 10–40%, depending on the location of interest (see green curves in lower panel of each

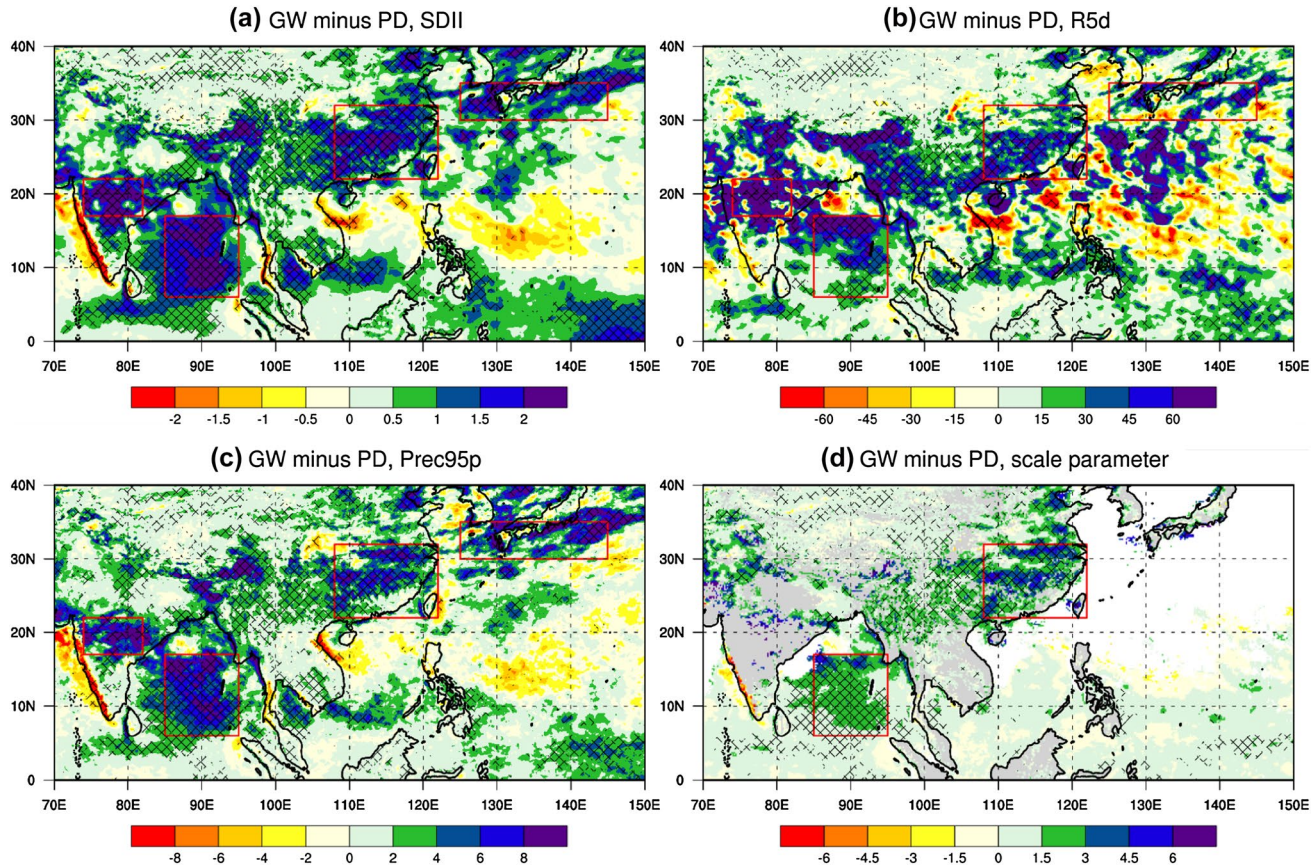

Fig. 5 Globally warmed-minus-present day of **a** SDII (units: mm day^{-1}), **b** R5d (units: mm), **c** Prec95p (units: mm day^{-1}) and **d** scale parameter (units: mm day^{-1}) for fitted gamma distributions of daily precipitation rates in MJJAS, based on MRI-AGCM simulations. For scale parameter, only grids with present-day non-zero precipitation PDF showing goodness of fit of gamma distribution for at least 80% of seasons (using K–S test at significance level = 0.1) are shown. Red boxes denote the sub-regions where coherent increases of both the mean and extreme precipitation are found, namely southeastern China (22–32N, 108–122E), Baiu rainband (30–35N, 125–145E), Bay of Bengal (6–17N, 85–95E) and central India (17–22N, 74–82E). Cross-hatches indicate that the differences pass the 90% significance level based on the two-sided Student's *t* test

Table 2 Globally-warmed minus present-day values of various statistics for the daily precipitation rate, averaged over different domains

	δMean (mm day^{-1})	δSDII (mm day^{-1})	δR5d (mm)	δPrec95p (mm day^{-1})	δScale (mm day^{-1})
Southeastern China (22–32N, 108–122E)	0.718 (4.45% K^{-1})	1.25 (5.40% K^{-1})	27.4 (7.27% K^{-1})	3.57 (4.68% K^{-1})	2.72 (7.83% K^{-1})
Baiu rainband (30–35N, 125–145E)	0.660 (3.33% K^{-1})	1.15 (3.69% K^{-1})	17.1 (3.48% K^{-1})	4.31 (3.32% K^{-1})	Not applicable
Bay of Bengal (6–17N, 85–95E)	1.58 (5.36% K^{-1})	1.76 (5.50% K^{-1})	37.3 (6.45% K^{-1})	5.77 (6.42% K^{-1})	2.05 (7.72% K^{-1})
Central India (17–22N, 74–82E)	1.24 (6.12% K^{-1})	2.02 (7.43% K^{-1})	83.9 (11.3% K^{-1})	6.89 (8.47% K^{-1})	Not applicable

Also shown are the same differences (in parentheses), divided by the corresponding regional changes in the MJJAS mean lower-tropospheric temperature. All projected changes of mean and precipitation extremes are statistically significant at the 99.9% level (Monte Carlo permutation test). Projected rate of extreme rainfall change per unit change of the lower-tropospheric temperature ranges from about 3.3 to 11% K^{-1}

figure). Both the SDII and Precp95p values also increase in these regions (see vertical lines in Fig. 6a–d). Statistical tests further testify that that the PDFs from the GW and PD experiments are indeed different in all four regions, significant to the 99.9% level (based on the K–S test). It is also notable that the increase in Precp95p is larger than that in SDII, such that the PDF for daily precipitation rates is becoming more right-skewed over all four regions under the influence of global warming.

In addition to comparing the empirically determined PDFs, daily rain rates for southeastern China and BOB, and their changes were also characterized using gamma

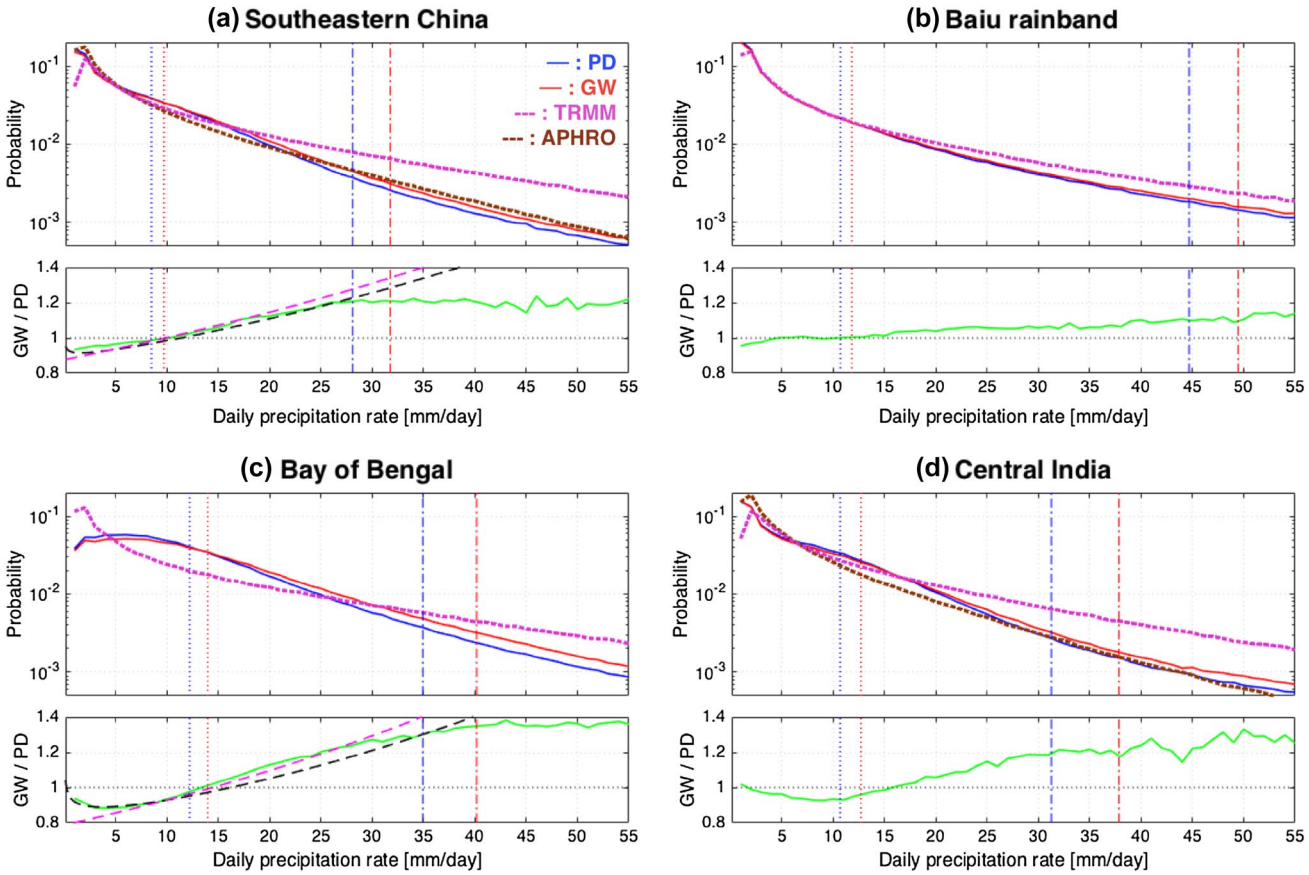

Fig. 6 Probability density function (PDF) for present-day (in solid blue) and globally-warmed (in solid red) daily precipitation rates, based on MRI-AGCM simulations from the sub-regions as indicated by red boxes in Fig. 5, namely **a** southeastern China (22–32N, 108–122E), **b** Baiu rainband (30–35N, 125–145E), **c** Bay of Bengal (6–17N, 85–95E) and **d** central India (17–22N, 74–82E). The observed PDFs for present-day daily precipitation rates based on TRMM-3B42V7 (dotted pink) and APHRODITEv1101 (dotted brown) are included for southeastern China and central India; for the Baiu rainband and Bay of Bengal regions, only those based on TRMM-3B42V7 are shown. Lower panel in each figure gives the globally-warmed PDF divided by the present-day PDF over each region (in solid green), with the fitted gamma distribution function in the globally-warmed future divided by that in present-day (in dashed black), and the same quantity estimated according to Eq. 3 (in dashed pink). The blue and red dotted (dot-dashed) vertical lines represent the present-day and globally-warmed SDII (Prec95p) respectively. See text for details

distributions. This can be done by first estimating the regionally-averaged shape and scale parameters, in both PD and GW experiments. Lower panels of Fig. 6a, c show the ratio of PDFs from GW to those from PD runs, computed based on fitted gamma distributions with the corresponding shape and scale parameters determined over southeastern China and BOB areas (see black dashed lines). It is seen that the ratio of PDFs based on parameterized distributions agrees well with that computed from the raw PDFs, at least up to the present-day 95th percentile values (around 30 mm day^{-1}) for both regions. Since the shape parameter only changes slightly (from 0.692 to 0.670, or a fractional change of -3.18% in southeastern China, and 1.30 to 1.24, i.e. a fractional change of -4.62%, in BOB), one may also assume that the shape parameter remains the same in the two AGCM experiments, to first approximation. Under such an assumption, the ratio of the PDF of GW to that of PD experiments can be approximated by:

$$\frac{f_{GW}}{f_{PD}} = \left(\frac{1}{c}\right)^{\alpha_{PD}} e^{\left(\frac{1}{\beta_{PD}}\right)\left(1-\frac{1}{c}\right)x} \tag{3}$$

where α_{PD} and β_{PD} are the present-day shape and scale parameters, and c is the scale parameter from GW divided by that from the PD experiment. It was found that β_{PD} over southeastern China (BOB) is 12.9 mm day^{-1} (10.1 mm day^{-1}), with an increase of 21.7% (20.8%) in the GW experiment. Using these estimates, we further examine whether it is valid to use the scale parameter alone to explain the changing PDF. By ignoring changes of the shape parameter (i.e. using Eq. 3), it can be seen that the fractional increase in extreme daily precipitation rates is overestimated (see pink dashed lines in lower panels of Fig. 6a, c). This is

especially obvious in southeastern China, and less so in BOB region. Thus, for characterizing changes in moderate precipitation extremes, the shape parameter can be assumed to be constant (such that Eq. 3 is valid). For very extreme values (say greater than 99th percentile), however, the gamma distribution seems not capable in representing their changes due to global warming; it always tends to overestimate the increase of probability for extremely heavy rainfall (compare black dashed with green curves Fig. 6a, c).

It is also instructive to compute the rate of change of extreme precipitation per unit degree of warming, and to compare such a rate at different locations with that predicted by the CC relation (see Sect. 1). Here the projected lower-tropospheric warming was estimated by the GW minus PD seasonal mean temperature, averaged over the 500–1000 hPa. Percentage changes of SDII, R5d and Precp95p divided by such temperature change were then computed at every grid point. The same quantity for the scale parameter is also included in southeastern China and BOB. The probability distributions of their gird point values over the four regions with robust precipitation increase are given in Fig. 7. It was found that over southeastern China, BOB and central India, changes in both the mean and extreme precipitation rates according to various metrics are in general agreement with the CC relation, i.e. the probability values generally peak around 7% K^{-1} (see dashed vertical line in panels); the exception is that, according to R5d, the change in central India gives a super-CC scaling. It is also noteworthy that both the mean and extreme rain rates seem to behave in the same manner under the global warming influence, except mean precipitation showing a weaker response as compared to extreme precipitation. Kusunoki and Mizuta (2013) also projected such weaker response of the mean relative to the extremes, and found that some areas of East Asia showed a super-CC scaling of R5d. However, over the Baiu rainband region, the most likely change in precipitation rates was found to be about 3.5% K^{-1} only. To reduce the uncertainty in estimating regional responses,

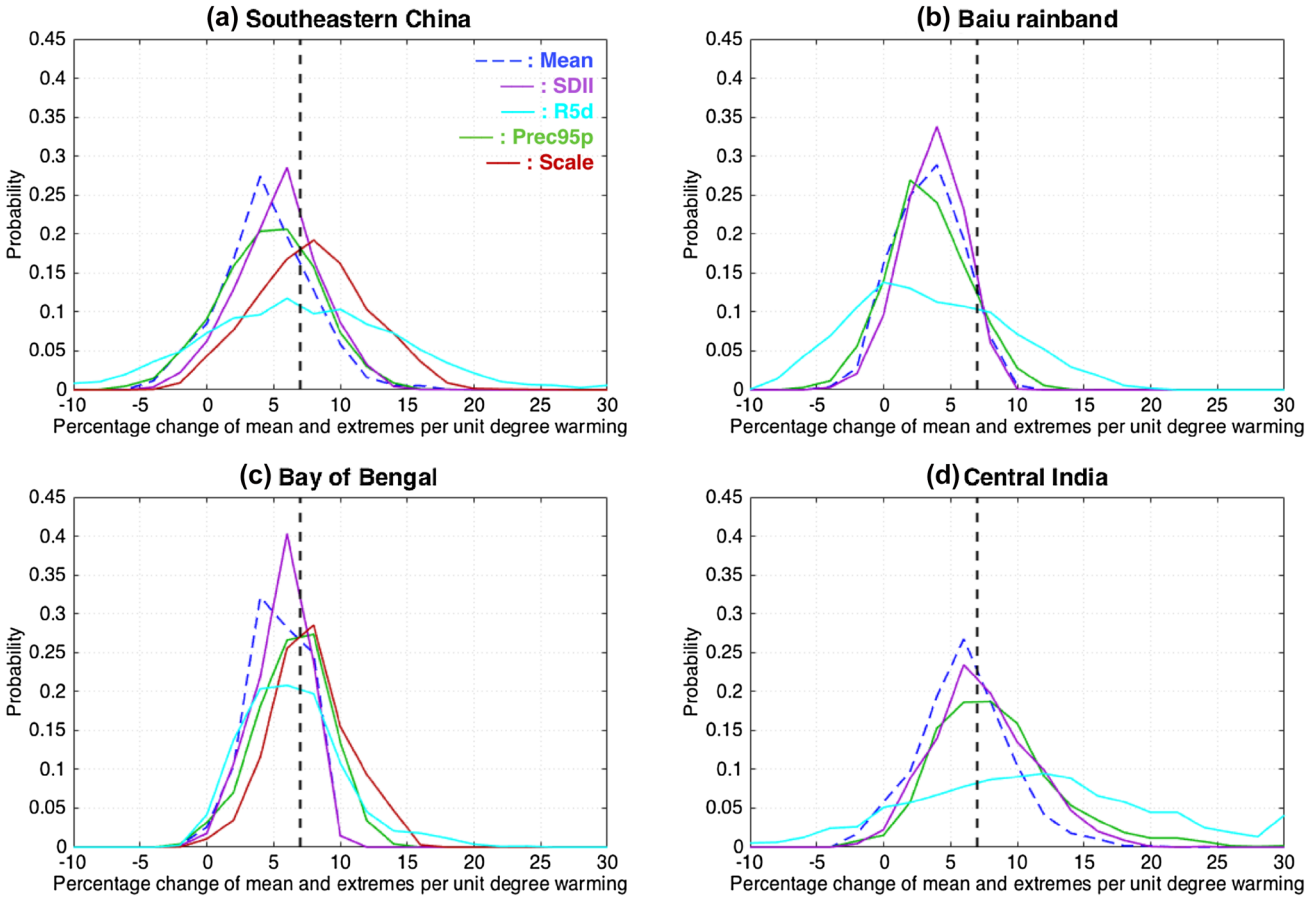

Fig. 7 Probability distribution of changes in the time mean precipitation rates (dotted blue line), SDII (purple), R5d (cyan), and Prec95p (green) per unit degree of warming in the lower-to-mid troposphere in MJJAS, in the globally-warmed compared to the present-day simulations, over grid boxes within **a** southeastern China (22–32N, 108–122E), **b** Baiu rainband (30–35N, 125–145E), **c** Bay of Bengal (6–17N, 85–95E) and **d** central India (17–22N, 74–82E), as indicated by the red boxes in Fig. 5. The probability distribution of changes in the scale parameter (red) for gamma-fitted daily precipitation rates, per unit degree of warming, is shown only for **a** southeastern China and **c** Bay of Bengal. The dashed vertical line denotes the Clausius–Clapeyron relation. See text for details

we have also taken the spatial average of the changes of these extreme indices per unit temperature change (see Fischer et al. 2013); the resulting values range from about 3.3 to 11% K^{-1} (Table 2). The area average of the projected change in daily mean precipitation rate per unit lower-tropospheric temperature change over MJJAS in the whole domain (0–60°N, 60–150°E) was found to be 3.05% K^{-1}.

5 Projected change in tropical cyclone rainfall

In this section the same sets of AGCM simulations were used to examine how climate change might influence TC precipitation over various East Asia locations. Figure 8a, b show the TCF in the GW experiments, as well as the GW minus PD TCF values, respectively. It is clear that there is an overall reduction of TC activity over the SCS and WNP regions, under the influence of global warming. TCF east and northeast of the Philippines is significantly affected, with a decrease about of 5–6 storm days per season (~45 to 50%). TC occurrences are also strongly suppressed over northwestern SCS near Vietnam and in southern Japan. Overall, there is a 25.6% reduction in TC genesis frequency in the WNP basin (not shown), which means about 9% less reduction than that given by Knutson et al. (2015). Inspection of the GW minus PD seasonal mean circulation revealed anomalous sinking motion in the mid-troposphere and low-level anti-cyclonic flow over SCS and east of the Philippines (see Figs. S4a and S4c). Furthermore, in the vicinity of southern Japan, there is enhanced vertical wind shear (see Fig. S4b). The above circulation changes are consistent with suppressed TC activity over these regions. We have also computed TC composites of the mean sea-level pressure (MSLP) and TC-related precipitation, for TCs identified in the PD and GW experiments. Figure 8c shows the azimuthally averaged results as a function of distance from the TC center, based on GW minus PD composites. The composite minimum SLP of a TC in the model is projected to decrease by ~85 Pa (~0.1%), while the rain rate will increase by up to 70 mm day^{-1} (~25% within 100 km) due to global warming; the latter is slightly larger than the fractional change in rain rate given by Knutson et al. (2015).

With increased TC rain rate but at the same time fewer TC storm days in the future GW climate, a question thus arises: how does the magnitude and geographical distribution of accumulated TC-related rainfall change accordingly?

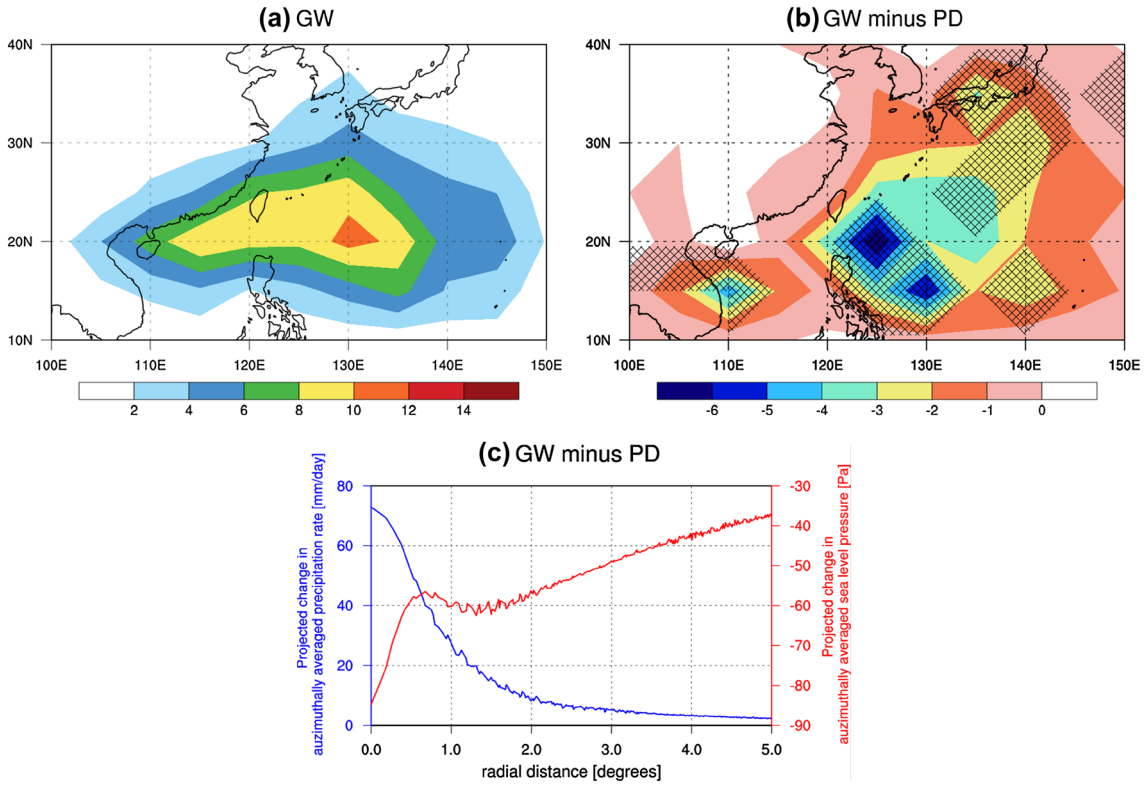

Fig. 8 **a** As in Fig. 4b but for future (globally warmed) climate simulations. **b** Globally-warmed minus present-day TC occurrence frequency per season over each 5° × 5° grid box in MJJAS. **c** Azimuthally averaged precipitation rate (blue, in units of mm day^{-1}) and MSLP (red, in units of Pa) as a function of distance from TC center, based on TC composites in the same season from MRI-AGCM simulations. Cross-hatches in **b** indicate that the differences pass the 90% significance level based on the two-sided Student's t test

Fig. 9a, b show the geographical distribution of TC-related accumulated rainfall from the PD and GW simulations; also shown is the difference between values from these two runs (Fig. 9c). It can be seen that there are robust changes in the accumulated TC rainfall over southeastern China (22–32N, 108–120E), and the Baiu rainband (30–35N, 125–145E). Such GW minus PD differences can be further written as the contributions from two terms, one due to change of TC rain rate and the other due to change of TC storm days as follows:

$$\begin{aligned}\delta TCP &= R_{GW}N_{GW} - R_{PD}N_{PD} \\ &= \frac{N_{GW}+N_{PD}}{2}(R_{GW}-R_{PD}) + \frac{R_{GW}+R_{PD}}{2}(N_{GW}-N_{PD}) \\ &= \bar{N}\delta R + R\delta N \end{aligned} \quad (4)$$

where R_{PD} and R_{GW} are the mean TC rain rates in mm day^{-1} in the PD and GW runs, respectively; N_{PD} (N_{GW}) denotes the mean TC storm days for the PD (GW) experiments. N and δN are the average and difference between N_{PD} and N_{GW} respectively; R and δR are defined similarly. These two components are calculated at every grid point and averaged over each geographical region. Their area averages as well as their sum total are presented in Fig. 9d. Despite the reduced numbers of storm days in southeastern China, having more precipitation per TC leads to an increase of accumulated rainfall by 12.4 mm per season, which corresponds to an increase of 0.0812 mm day^{-1} in the mean rainfall (see Tables 2, 3). In contrast, the accumulated TC rainfall is projected to decrease by 25.5 mm per season (i.e. 0.167 mm day^{-1}) over the Baiu region, which is mainly due

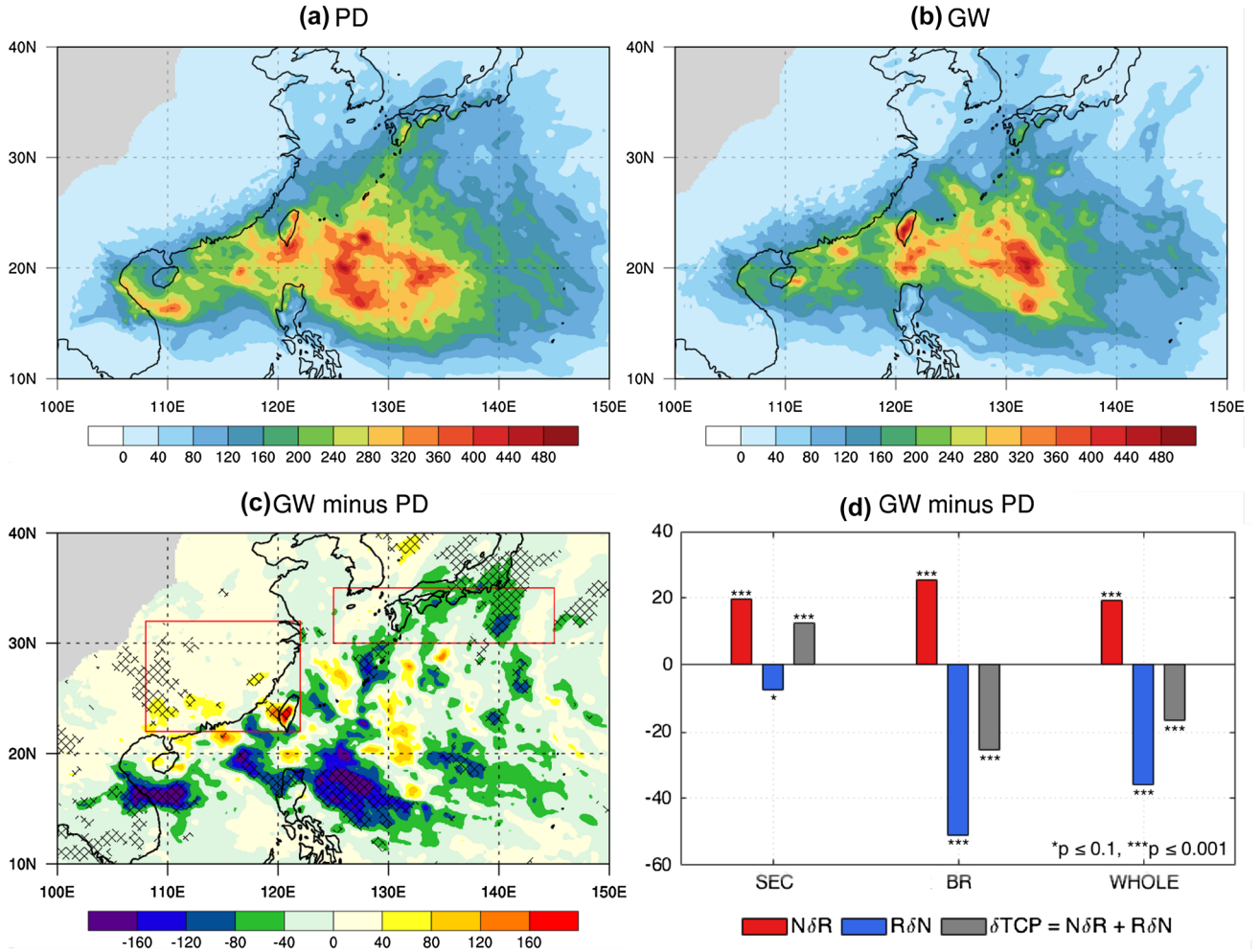

Fig. 9 **a** Present-day, **b** globally-warmed future accumulated TC rainfall per season in MJJAS based on MRI-AGCM simulations. **c** Difference between **b** and **a** (units: mm). **d** Globally-warmed minus present-day accumulated TC rainfall per MJJAS season due to change of TC intensity (red), due to change of TC storm days (blue) and their sum (grey) based on MRI-AGCM simulations, for southeastern China (SEC; 22–32N, 108–122E), Baiu rainband (BR; 30–35N, 125–145E), and the whole domain (WHOLE; 10–40N, 100–150E). Red boxes in **c** denote the sub-regions for southeastern China and Baiu rainband. Cross-hatches in **c** indicate that the differences pass the 90% significance level based on the two-sided Student's t test. Asterisks over bars in **d** indicate the p value of the results based on the two-sided Student's t test (see convention at bottom right)

Table 3 As in Table 2 but statistics are computed based on non-TC related daily precipitation

	δMean (mm day^{-1})	δSDII (mm day^{-1})	δR5d (mm)	δPrec95p (mm day^{-1})
Southeastern China (22–32N, 108–122E)	0.637	1.14	21.4	3.45
Baiu rainband (30–35N, 125–145E)	0.827	1.35	22.8	5.32

to the reduction of storm days there. On average, the accumulated TC rainfall per season is projected to decrease by 16.5 mm over the domain of 10°–40°N, 100°–150°E.

Finally, we investigate how TC-related precipitation change might contribute to the overall change of extreme precipitation in these two regions. In particular, we have further stratified rainfall rates into five categories, namely those within 0.1–1, 1–10, 10–50, 50–200 and more than 200 mm day^{-1}, and for TC and non-TC related events separately. Figure 10 gives the GW minus PD number of TC and non-TC related rainfall events per season over southeastern China and the Baiu region. Based on the AGCM simulations, the overall non-TC (TC) rainfall frequency over southeastern China and Baiu region will decrease by 2.10% (5.28%) and 0.277% (36.9%) in the globally-warmed future, respectively. Despite the overall decrease in non-TC rainfall frequency, the likelihood of non-TC events with rain rates greater than 10 mm day^{-1} is projected to increase by ~2 days per season in both regions under the global warming influence (see Fig. 10), meaning an intensification of precipitation extremes. In contrast, future changes of TC-related precipitation as a function of intensity differ substantially in the two regions, and so do their effects on extreme precipitation. For southeastern China, there is an increase (decrease) of the occurrence of more (less) intense TC-related precipitation events with rain rates greater (smaller) than 50 mm day^{-1} (Fig. 10a). On the other hand, the probability of TC-related events is projected to decrease regardless of their intensity over the Baiu region (Fig. 10b), which is consistent with the significant reduction of TC activity in this region (see again Fig. 8b). To quantify the contributions of TC-related rainfall changes to the overall precipitation statistics, we first removed the TC-related events and computed the changes of the non-TC precipitation statistics in these two regions (Table 3). Then, we calculated the corresponding percentage changes by comparing them to those in Table 2 as follows:

$$\%\ \text{change} = \frac{\delta X_{nTC+TC} - \delta X_{nTC}}{\left|\delta X_{nTC}\right|} \times 100\% \tag{5}$$

where δX_{nTC+TC} and δX_{nTC} are the future changes of the precipitation indices without and with TC-related rainfall removed, respectively. In southeastern China, the computed changes in R5d and Prec95p based on non-TC rainfall events are 21.4 mm and 3.45 mm day^{-1} respectively, which are smaller than those without removing TC rainfall (27.4 mm and 3.57 mm day^{-1}), suggesting that TC-related rainfall changes will further intensify the two extreme indices by 28.0 and 3.48% respectively (Table 4). In contrast, in the Baiu region, changes in R5d and Prec95p based on non-TC rainfall events are 22.8 mm and 5.32 mm day^{-1} respectively, which are larger than those without removing TC rainfall (17.1 mm and 4.31 mm day^{-1} respectively); this means that TC-related rainfall changes will act to reduce the two

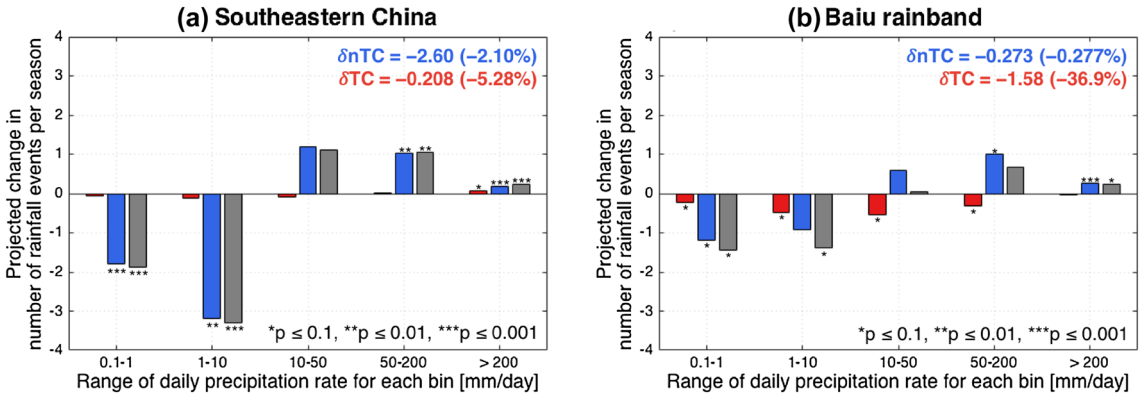

Fig. 10 Globally-warmed minus present-day TC (red), non-TC (blue) rainfall event number per season, as well as their sum total (grey), as a function of daily precipitation intensities, over **a** southeastern China (22–32N, 108–122E), and **b** Baiu rainband (30–35N, 125–145E). The overall change in number (and percentage change in parentheses) of non-TC and TC related rainfall events is shown in the upper right of each figure. Asterisks over bars indicate the p value of the results based on the two-sided Student's t test (see convention at bottom right). See text for details

Table 4 Percentage changes of the statistics in Table 3, if the future change of TC-related rainfall is also taken into account

	δMean (%)	δSDII	δR5d	δPrec95p
Southeastern China (22–32N, 108–122E)	+12.7	+9.65	+28.0	+3.48
Baiu rainband (30–35N, 125–145E)	− 20.2	− 14.8	− 25.0	− 19.0

See text for details

extreme indices by 25.0 and 19.0% respectively (Table 4). Overall, non-TC weather systems plays a more important role, as compared to TCs, in exacerbating the daily precipitation extremes in both regions under global warming. An increase in TC-related extreme precipitation in southeastern China tends to further exacerbate the precipitation extremes there, but a reduction in TC-related extreme precipitation in the Baiu region will partially offset such exacerbation.

6 Discussion and conclusion

We have assessed the performance of the MRI AGCM version 3.2S in simulating extreme precipitation- including that induced by TCs- in boreal summer over the Asian monsoon region, and have examined how global warming might influence these extremes in the model environment. Overall, the AGCM performs well in capturing the seasonal mean as well as extreme precipitation patterns in Southeast and East Asia. The model daily precipitation extremes are fairly consistent with those based on APHRODITE data over land areas, but less than those given by the TRMM dataset. By comparing the GW with PD experiments, the summertime mean rain rate is projected to increase over many locations in the Asian monsoon region. Note that when discussing the impacts of climate change on the Asian monsoon, one should differentiate between changes in the wind circulation and those in the monsoon rainfall. Here it was found that the monsoon rainfall is enhanced in general, despite weakened low-level westerlies over the tropical Indian Ocean and SCS under the influence of global warming.

Over the regions of southeastern China, the Baiu rainbelt, BOB, and central India there are robust increase in both the seasonal mean precipitation and extreme rainfall. Summertime mean daily (95th percentile) rain rates over these areas are projected to increase by about 0.7–1.6 (3.6–6.9) mm day^{-1}. Further inspection revealed that PDFs for daily precipitation in these regions from the GW runs are significantly different from their PD counterparts, with the greatest increase in probability found in the higher percentiles. We have also investigated the model precipitation characteristics in different Asia monsoon regions using the parametric gamma function. It was found that PDFs of daily rain rates over southeastern China and BOB can be well represented by the gamma distribution. Such an parametric approach was then used to study how global warming might impact on precipitation behavior in these two regions. There is robust increase of the scale parameter in the two regions (21.7 and 20.8% in southeastern China and BOB, respectively), leading to enhanced probability precipitation rates in the higher percentiles. Slight reductions of the shape parameters were also found (− 3.18 and −4.62% in southeastern China and BOB respectively). It appears that the gamma fitting provides a concise way to describe the change of daily rain rates, accurate up to about the 95th percentile. For even more extreme precipitation events, however, the gamma distribution tends to overestimate the change of their occurrence frequency compared to that computed based on the actual PDFs.

We have also compared the increment of extreme rainfall due to global warming with that given by the CC relation. Based on the model-projected increase of about 2.98 K in the MJJAS mean lower-tropospheric air temperature, changes of precipitation extremes per unit change of the local lower-tropospheric temperature were computed. In three out of four aforementioned domains with robust increase of extreme rain rates, namely southeastern China, BOB and central India, the results are about 4.7 to 8.5% K^{-1}, which are roughly consistent with the CC relation (except that R5d gives a change of 11.3% K^{-1} over central India). However, over south of Japan in the Baiu region, the change is only about 3.5% K^{-1}. In fact, we have checked that the model precipitable water increases by about 6–7% K^{-1} in the same region (see Fig. S3). This suggests that the relatively modest increase of extreme rain rates is not due to limitations in the amount of precipitable water; instead, dynamic changes such as those in monsoon circulation might play an important role in this region. Chu et al. (2012) and Oh and Ha (2015) have shown that intense rainfall for the Meiyu–Baiu mode is more strongly related to dynamical factors such as anomalous low-level convergence and vertical wind shear, than thermodynamic factors. In our study, an enhanced vertical zonal wind shear is projected near this region (Fig. S4b), which might be the reason for the sub-CC scaling of extreme precipitation for the model. Further study is needed to unveil if this or other dynamical factors are responsible for the sub-CC scaling in this region. In this study we also seek to understand how large-scale circulation might change and subsequently how it might strengthen or weaken regional extreme rainfall under warming climate, although previous studies have already shown dynamic factors might play a big role in inducing extreme rainfall over some Asian monsoon sub-regions.

We have also investigated how TC-related rainfall might be influenced by global warming. There is an overall reduction of TC numbers over the WNP basin, when comparing GW with PD experiments. This is likely due to the reduced low-level relative vorticity over a broad area in this domain; also, the variance of high-frequent vorticity fluctuations is reduced east of the Philippines and part of SCS (figure not shown). On the other hand, TC-related rain rate is projected to increase, in conjunction with TCs becoming more intense in a warmer climate. Overall, the combined effect of these two competing factors leads to more (less) TC rainfall over southeastern China and northern SCS (east of the Philippines and southern Japan). Further analyses indicated that indeed the reduced TC-related rainfall in southern Japan can be attributed to the suppression of TC activity there; the increased TC-related rainfall over southeastern China is due to more intense TC rain rate. Finally, by analyzing TC and non-TC related rainfall data, it was found that the enhanced daily precipitation extremes cover many locations can be mainly attributed to non-TC weather systems. In southeastern China, both TC and non-TC related rainfall events contribute to the increase of extremes, with the latter weather type being the main contributor. For the Baiu rainband, there is also an increase of the frequency of the most intense precipitation; this is again due to non-TC rainfall, while TCs are expected to partially offset such increase.

Finally, the above assessment on TC-related mean and extreme precipitation changes might be affected by uncertainties in the projected TC characteristics (such as TC tracks), and by the relatively small sampling size of TC precipitation events. Over various sub-domains, the extreme rain rate from this AGCM, although matches reasonably with those from APHRODITE, seems to be underestimated compared to TRMM. It is unclear why there is such a disagreement between APHRODITE and TRMM in this aspect; thus the future projection of extreme precipitation given by this model needs to be considered with caution. Recently, Kitoh and Endo (2016b) and Endo et al. (2017) analysed future changes in precipitation extremes related to El Nino and TCs, using the same AGCM. It was found that the interannual variability of precipitation extreme will also increase, besides the climatological mean of extremes. The uncertainty of model physics (e.g. the cumulus scheme) as well as that in the SST field can contribute significantly to the uncertainty of changes in precipitation extremes in East Asia/WNP. Furthermore, Kusunoki (2017a) found that the version and resolution of the AGCM can also add uncertainty to the geographical distribution of extreme precipitation changes, although the broad-scale changes of extreme precipitation over East Asia are generally consistent among similar studies. Apparently, more studies are needed to ascertain future characteristics of TCs, intense precipitation, and for understanding their relationship with different climate phenomena, by conducting and analysing various high-resolution model climate projections for the Asian monsoon area.

Acknowledgements The authors would like to thank Dr. Akio Kitoh for generous sharing the MRI-AGCM outputs from the KAKUSHIN Program, and Profs. C.P. Chang, Kyung-Ja Ha, June-Yi Lee and Song Yang for discussions. Comments from the anonymous reviewers help to strengthen this work. NCL at the Chinese University of Hong Kong is supported by the AXA Research Fund.

References

Alexander LV, Zhang X, Peterson TC et al (2006) Global observed changes in daily climate extremes of temperature and precipitation. J Geophys Res Atmos 111:1–22. https://doi.org/10.1029/2005JD006290

Allen MR, Ingram WJ (2002) Constraints on future changes in climate and the hydrologic cycle. Nature 419:224–232. https://doi.org/10.1038/nature01092

Chang CP, Lei Y, Sui CH et al (2012) Tropical cyclone and extreme rainfall trends in East Asian summer monsoon since mid-20th century. Geophys Res Lett 39:1–6. https://doi.org/10.1029/2012GL052945

Chen C-S, Chen Y-L, Liu C-L et al (2007) Statistics of heavy rainfall occurrences in Taiwan. Weather Forecast 22:981–1002. https://doi.org/10.1175/WAF1033.1

Cho H-K, Bowman KP, North GR (2004) A comparison of gamma and lognormal distributions for characterizing satellite rain rates from the tropical rainfall measuring mission. J Appl Meteorol 43:1586–1597. https://doi.org/10.1175/JAM2165.1

Chu J-E, Hameed SN, Ha K-J (2012) Nonlinear, intraseasonal phases of the East Asian summer monsoon: extraction and analysis using self-organizing maps. J Clim 25:6975–6988. https://doi.org/10.1175/JCLI-D-11-00512.1

Donat MG, Lowry AL, Alexander LV et al (2016) More extreme precipitation in the world's dry and wet regions. Nat Clim Change 6:508–513. https://doi.org/10.1038/nclimate2941

Easterling DR (2000) Climate extremes: observations, modeling, and impacts. Science (80) 289:2068–2074. https://doi.org/10.1126/science.289.5487.2068

Emanuel KA (2013) Downscaling CMIP5 climate models shows increased tropical cyclone activity over the 21st century. Proc Natl Acad Sci 110:12219–12224. https://doi.org/10.1073/pnas.1301293110

Emori S, Brown SJ (2005) Dynamic and thermodynamic changes in mean and extreme precipitation under changed climate. Geophys Res Lett 32:1–5. https://doi.org/10.1029/2005GL023272

Endo H, Kitoh A, Ose T et al (2012) Future changes and uncertainties in Asian precipitation simulated by multiphysics and multi-sea surface temperature ensemble experiments with high-resolution Meteorological Research Institute atmospheric general circulation models (MRI-AGCMs). J Geophys Res Atmos. https://doi.org/10.1029/2012JD017874

Endo H, Kitoh A, Mizuta R, Ishii M (2017) Future changes in precipitation extremes in East Asia and their uncertainty based on large ensemble simulations with a high-resolution AGCM. Sola 13:7–12. https://doi.org/10.2151/sola.2017-002

Field CB, Barros V, Stocker TF, Qin D, Dokken DJ, Ebi KL, Mastrandrea MD, Mach KJ, Plattner G-K, Allen SK, Tignor M, Midgley PM (eds.) (2012) Managing the risks of extreme events and disasters to advance climate change adaptation. A special report of

working groups I and II of the intergovernmental panel on climate change. Cambridge University Press, Cambridge (IPCC)
Fischer EM, Beyerle U, Knutti R (2013) Robust spatially aggregated projections of climate extremes. Nat Clim Change 3:1033–1038. https://doi.org/10.1038/nclimate2051
Frich P, Alexander LV, Della-Marta P et al (2002) Observed coherent changes in climatic extremes during the second half of the twentieth century. Clim Res 19:193–212. https://doi.org/10.3354/cr019193
Fujibe F (2013) Clausius–Clapeyron-like relationship in multidecadal changes of extreme short-term precipitation and temperature in Japan. Atmos Sci Lett 14:127–132. https://doi.org/10.1002/asl2.428
Groisman PY, Karl TR, Easterling DR et al (1999) Changes in the probability of heavy precipitation: Important indicators of climatic change. Clim Change 42:243–283
Groisman PY, Knight RW, Easterling DR et al (2005) Trends in intense precipitation in the climate record. J Clim 18:1326–1350. https://doi.org/10.1175/JCLI3339.1
Guo L, Klingaman NP, Vidale PL et al (2017) Contribution of tropical cyclones to atmospheric moisture transport and rainfall over East Asia. J Clim. https://doi.org/10.1175/JCLI-D-16-0308.1
Hirai M, Sakashita T, Kitagawa H, Tsuyuki T (2007) Development and validation of a new land surface model for JMA's operational global model using the CEOP observation dataset. J Meteorol Soc Jpn 85:1–24. https://doi.org/10.2151/jmsj.85A.1
Huffman GJ, Bolvin DT, Nelkin EJ et al (2007) The TRMM multisatellite precipitation analysis (TMPA): quasi-global, multiyear, combined-sensor precipitation estimates at fine scales. J Hydrometeorol 8:38–55. https://doi.org/10.1175/JHM560.1
Japan Meteorological Agency (2007) Outline of the operational numerical weather prediction at the Japan Meteorological Agency (appendix to WMO numerical weather prediction progress report). Japan Meteorological Agency, p 194. http://www.jma.go.jp/jma/jma-eng/jmacenter/nwp/outline-nwp/index.htm
Jiang H, Zipser EJ (2010) Contribution of tropical cyclones to the global precipitation from eight seasons of TRMM data: regional, seasonal, and interannual variations. J Clim 23:1526–1543. https://doi.org/10.1175/2009JCLI3303.1
Jiang Z, Song J, Li L et al (2012) Extreme climate events in China: IPCC-AR4 model evaluation and projection. Clim Change 110:385–401. https://doi.org/10.1007/s10584-011-0090-0
Kamiguchi K, Arakawa O, Kitoh A et al (2010) Development of APHRO_JP, the first Japanese high-resolution daily precipitation product for more than 100 years. Hydrol Res Lett 4:60–64. https://doi.org/10.3178/hrl.4.60
Kitoh A, Endo H (2016a) Changes in precipitation extremes projected by a 20-km mesh global atmospheric model. Weather Clim Extrem 11:41–52. https://doi.org/10.1016/j.wace.2015.09.001
Kitoh A, Endo H (2016b) Future changes in rainfall extremes associated with El Niño projected by a global 20-km mesh atmospheric model. Sola 12A:1–6. https://doi.org/10.2151/sola.12A-001
Knutson TR, McBride JL, Chan J et al (2010) Tropical cyclones and climate change. Nat Geosci 3:157–163. https://doi.org/10.1038/ngeo779
Knutson TR, Sirutis JJ, Zhao M et al (2015) Global projections of intense tropical cyclone activity for the late twenty-first century from dynamical downscaling of CMIP5/RCP4.5 scenarios. J Clim 28:7203–7224. https://doi.org/10.1175/JCLI-D-15-0129.1
Kobayashi S, Ota Y, Harada Y et al (2015) The JRA-55 reanalysis: general specifications and basic characteristics. J Meteorol Soc Jpn Ser II 93:5–48. https://doi.org/10.2151/jmsj.2015-001
Kossin JP, Emanuel KA, Camargo SJ (2016) Past and projected changes in western north pacific tropical cyclone exposure. J Clim 29:5725–5739. https://doi.org/10.1175/JCLI-D-16-0076.1
Kusunoki S (2016) Is the global atmospheric model MRI-AGCM3. 2 better than the CMIP5 atmospheric models in simulating precipitation over East Asia ? Clim Dyn. https://doi.org/10.1007/s00382-016-3335-9
Kusunoki S (2017a) Future changes in precipitation over East Asia projected by the global atmospheric model MRI-AGCM3.2. Clim Dyn 9:1–17. https://doi.org/10.1007/s00382-016-3499-3
Kusunoki S (2017b) Future changes in global precipitation projected by the atmospheric model MRI-AGCM3.2H with a 60-km size. Atmosphere (Basel) 8:93. https://doi.org/10.3390/atmos8050093
Kusunoki S, Mizuta R (2013) Changes in precipitation intensity over East Asia during the 20th and 21st centuries simulated by a global atmospheric model with a 60 km grid size. J Geophys Res Atmos 118:11007–11016. https://doi.org/10.1002/jgrd.50877
Lau K-M, Wu H-T (2007) Detecting trends in tropical rainfall characteristics, 1979–2003. Int J Climatol 27:979–988. https://doi.org/10.1002/joc
Lenderink G, van Meijgaard E (2008) Increase in hourly precipitation extremes beyond expectations from temperature changes. Nat Geosci 1:511–514. https://doi.org/10.1038/ngeo262
Manganello JV, Hodges KI, Dirmeyer B et al (2014) Future changes in the western North Pacific tropical cyclone activity projected by a multidecadal simulation with a 16-km global atmospheric GCM. J Clim 27:7622–7646. https://doi.org/10.1175/JCLI-D-13-00678.1
Meehl GA, Zwiers F, Evans J et al (2000) Trends in extreme weather and climate events: Issues related to modeling extremes in projections of future climate change. Bull Am Meteorol Soc 81:427–436. https://doi.org/10.1175/1520-0477(2000)0812.3.co;2
Mellor GL, Yamada T (1974) A hierarchy of turbulence closure models for planetary boundary layers. J Atmos Sci 31:1791–1806
Mizuta R, Yoshimura H, Endo H et al (2012) Climate simulations using MRI-AGCM3.2 with 20-km grid. J Meteorol Soc Jpn 90:233–258. https://doi.org/10.2151/jmsj.2012-A12
Murakami H, Wang B, Kitoh A (2011) Future change of western North Pacific typhoons: projections by a 20-km-mesh global atmospheric model. J Clim 24:1154–1169. https://doi.org/10.1175/2010JCLI3723.1
Murakami H, Wang Y, Yoshimura H et al (2012) Future changes in tropical cyclone activity projected by the new high-resolution MRI-AGCM. J Clim 25:3237–3260. https://doi.org/10.1175/JCLI-D-11-00415.1
Oh H, Ha KJ (2015) Thermodynamic characteristics and responses to ENSO of dominant intraseasonal modes in the East Asian summer monsoon. Clim Dyn 44:1751–1766. https://doi.org/10.1007/s00382-014-2268-4
Pall P, Allen MR, Stone DA (2007) Testing the Clausius–Clapeyron constraint on changes in extreme precipitation under CO_2 warming. Clim Dyn 28:351–363. https://doi.org/10.1007/s00382-006-0180-2
Qian W, Lin X (2005) Regional trends in recent precipitation indices in China. Meteorol Atmos Phys 90:193–207. https://doi.org/10.1007/s00703-004-0101-z
Rayner NA, Parker DE, Horton EB et al (2003) Global analyses of sea surface temperature, sea ice, and night marine air temperature since the late nineteenth century. J Geophys Res 108:4407. https://doi.org/10.1029/2002JD002670
Semenov V, Bengtsson L (2002) Secular trends in daily precipitation characteristics: Greenhouse gas simulation with a coupled AOGCM. Clim Dyn 19:123–140. https://doi.org/10.1007/s00382-001-0218-4
Sillmann J, Roeckner E (2008) Indices for extreme events in projections of anthropogenic climate change. Clim Change 86:83–104. https://doi.org/10.1007/s10584-007-9308-6
Sillmann J, Kharin VV, Zwiers FW et al (2013) Climate extremes indices in the CMIP5 multimodel ensemble: Part 2. Future climate

projections. J Geophys Res Atmos 118:2473–2493. https://doi.org/10.1002/jgrd.50188
Sohn SJ, Tam CY, Ashok K, Ahn JB (2012) Quantifying the reliability of precipitation datasets for monitoring large-scale East Asian precipitation variations. Int J Climatol 32:1520–1526. https://doi.org/10.1002/joc.2380
Solomon S, Qin D, Manning M et al (2007) Climate change 2007-the physical science basis: Working group I contribution to the fourth assessment report of the IPCC. Cambridge University Press, Cambridge
Sugi M, Murakami H, Yoshimura J (2009) A reduction in global tropical cyclone frequency due to global warming. Sola 5:164–167. https://doi.org/10.2151/sola.2009-042
Sun Y, Solomon S, Dai A, Portmann RW (2007) How often will it rain? J Clim 20:4801–4818. https://doi.org/10.1175/JCLI4263.1
Vecchi GA, Soden BJ (2007) Global warming and the weakening of the tropical circulation. J Clim 20:4316–4340. https://doi.org/10.1175/JCLI4258.1
Wang Y, Zhou L (2005) Observed trends in extreme precipitation events in China during 1961–2001 and the associated changes in large-scale circulation. Geophys Res Lett 32:1–4. https://doi.org/10.1029/2005GL022574
Wilby RL, Wigley TML (2002) Future changes in the distribution of daily precipitation totals across North America. Geophys Res Lett 29:1135. https://doi.org/10.1029/2001gl013048
Xie P, Yatagai A, Chen M et al (2007) A gauge-based analysis of daily precipitation over East Asia. J Hydrometeorol 8:607–626. https://doi.org/10.1175/JHM583.1
Yatagai A, Yasutomi N, Hamada A et al (2012) APHRODITE: constructing a long-term daily gridded precipitation dataset for Asia based on a dense network of rain gauges. Bull Am Meteorol Soc 14:6995. https://doi.org/10.1175/BAMS-D-11-00122.1
Yokoi S, Takayabu YN, Chan JCL (2009) Tropical cyclone genesis frequency over the western North Pacific simulated in medium-resolution coupled general circulation models. Clim Dyn 33:665–683. https://doi.org/10.1007/s00382-009-0593-9
Yukimoto S, Yoshimura H, Hosaka M et al (2011) Meteorological Research Institute—earth system model version 1 (MRI-ESM1). Tech Rep 64:88. https://doi.org/10.11483/mritechrepo.64
Yun K-S, Shin S-H, Ha K-J et al (2008) East Asian precipitation change in the global warming climate simulated by a 20-km mesh ACGM. Asia Pac J Atmos Sci 44:233–247
Zhai P, Zhang X, Wan H, Pan X (2005) Trends in total precipitation and frequency of daily precipitation extremes over China. J Clim 18:1096–1108. https://doi.org/10.1175/JCLI-3318.1
Zhang X, Alexander L, Hegerl GC et al (2011) Indices for monitoring changes in extremes based on daily temperature and precipitation data. Wiley Interdiscip Rev Clim Chang 2:851–870. https://doi.org/10.1002/wcc.147
Zhao T, Yatagai A (2014) Evaluation of TRMM 3B42 product using a new gauge-based analysis of daily precipitation over China. Int J Climatol 2762:2749–2762. https://doi.org/10.1002/joc.3872